



1

2

3

4 **Modeling and observing the Lake Albano dynamics**

5 Authors:

6 **Anita Grezio¹, Damiano Delrosso¹, Marco Anzidei², Marco Bianucci³, Giovanni
7 Chiodini¹, Antonio Costa¹, Antonio Guarnieri¹, Marina Locritani⁴, Silvia Merlini³,
8 Filippo Muccini⁴, Marco Paterni³, Dmitri Rouwet¹, Giancarlo Tamburello¹, Georg
9 Umgiesser^{5,6}**

10 ¹ Istituto Nazionale di Geofisica e Vulcanologia, Bologna, Italy

11 ² Istituto Nazionale di Geofisica e Vulcanologia, Roma, Italy

12 ³ CNR, Lerici, Italy

13 ⁴ Istituto Nazionale di Geofisica e Vulcanologia, Roma2, Italy

14 ⁵ ISMAR-CNR, Venezia, Italy

15 ⁶ Klaipeda University, Klaipeda, Lithuania

16 Corresponding author: anita.grezio@ingv.it, <https://orcid.org/0000-0001-6848-7589>

17

18 **Abstract**

19 Lake Albano is a monomictic volcanic crater lake in Central Italy with CO₂-rich waters
20 presenting CO₂ concentration varying over time. Depending on the period of the year, the
21 lake is characterized by strong stratification or rather overturning events. In the warm season,
22 the heating of the surface water results in a highly stratified vertical density profile, while in
23 the cold season, the surface water cooling leads to a potential vertical instability of the water
24 column. In this case, a partial/deep overturning of the lake water column may occur with the
25 degassing in the atmosphere of the CO₂ which was accumulated as dissolved species in the
26 deep water layers following seismically induced gas recharge, months to years before. Such a
27 process has been periodically observed in Lake Albano in the past and could pose a potential
28 hazard to the surrounding environment and population. A 3D numerical model is
29 implemented to investigate the lake dynamics and the occurrence of overturning events. The
30 model is validated and calibrated using both historical observations and measurements
31 acquired during this study. These include temperature and salinity profiles from the deepest
32 central portion of the lake, surface water temperature time series recorded by sensors installed
33 on the lake shores, mounted on remotely operated vehicles, and on low-cost, innovative, self-
34 powered drifting buoys. The latter have also been used to assess the modeled surface
35 circulation of the lake.

36



37 1. Introduction

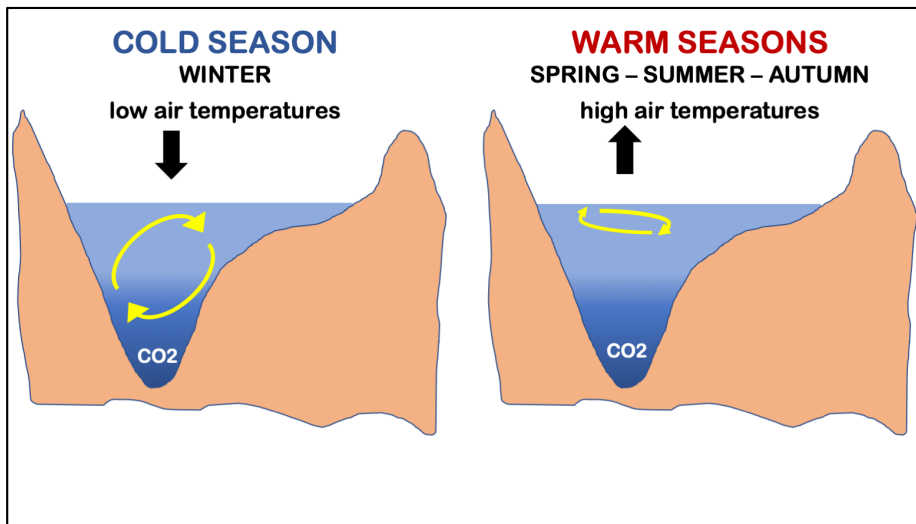
38 After the limnic eruption of Lake Nyos in 1986 (Kanari 1989; Kling et al. 1989), volcanic
39 lakes have been recognized as a rare but devastating source of disasters (Kusakabe 2017,
40 Kling et al. 2015). Limnic eruptions are caused by the accumulation of magmatic CO₂ in non-
41 acidic crater lakes, reaching supersaturation, or triggered by an external factor (e.g.
42 earthquake, landslide, strong winds). The gas recharge might occur for two reasons: a) a
43 sudden injection through the lake bottom of a relevant quantity of CO₂, or b) a high CO₂
44 concentration built up within the lake for a long time (Rouwet et al. 2019).

45 Italy hosts twelve volcanic lakes (Albano, Nemi, Averno, Lucrino, the two Monticchio lakes,
46 Bolsena, Bracciano, Vico, Mezzano, Martignano, Monterosi, Specchio di Venere-Pantelleria,
47 Telese) with different physical and chemical characteristics (Cioni et al. 2003; Chiodini et al.
48 2000; Chiodini et al. 2004; Stoch et al. 2007). The Albano maar is the deepest among the
49 volcanic crater lakes of Italy, being about 167 m deep (in 2007, see Anzidei et al., 2007). It is
50 the youngest of the monogenetic and polygenetic phreatomagmatic craters located along the
51 northern and the western slopes of the Colli Albani volcanic complex (De Rita et al. 1987; De
52 Rita et al. 1988; Trigila 1995; Villa et al. 1999; Funiciello et al. 2003; Marra et al. 2003; Freda
53 et al. 2006; Giordano et al. 2010). The lake has a long history of level changes and
54 catastrophic events, which started with the formation of the Albano crater ~70 ka B.P., and
55 continued during pre-historical times. Geological and historical evidence suggests that a large
56 overflow of the lake occurred in 396 B.C.E. due to a rapid increase of the water level. The
57 event contributed to fill the valleys on the north flank of the Albano maar crater forming the
58 Tavolato di Ciampino, an area characterized by a flat topography which is presently the site
59 of the international airport (Funiciello et al. 2003). In Lake Albano, a water overturning or a
60 mixing of deep and shallow waters could bring CO₂ from the bottom of the lake to the
61 surface with a potentially hazardous release of CO₂ (Funiciello et al. 2003; Carapezza et al.
62 2008; Chiodini et al. 2012). Such overturns may occur when the equilibrium of the water-
63 column stratification is modified by water density variations. The potential risk of Lake
64 Albano (20 km southeast of the centre of Rome) is due to exposed elements (people presence,
65 economic and touristic activities). As such, to estimate the potential gas hazard of Lake
66 Albano, numerical modeling of the lake water dynamics is crucial for understanding its
67 current and future behavior and stability.

68 In 1989, Lake Albano was affected by a large CO₂ input pulse during a seismic swarm below
69 Colli Albani volcano. On the basis of historical literature, at least two similar anomalous
70 degassing events took place between 1829 and 1927, when five seismic crises occurred
71 (Rouwet et al. 2019). A recent (August 2020), short seismic swarm resulted in a minor CO₂
72 recharge in deep water layers (Rouwet et al. in prep.). Apart from those significant episodes,
73 a moderate degassing of likely magmatic origin is present at irregular intervals. Lake Albano
74 is considered a monomictic lake and almost every winter, during the water overturning
75 (**Figure 1**) the lake commonly releases CO₂ (Chiodini et al. 2012) in non-hazardous amounts,
76 thereby preventing long-term CO₂ accumulation in the bottom waters. This is in contrast to
77 the dynamics of tropical stratified lakes, such as Lake Nyos (Rouwet et al. 2021), where lake
78 overturn does not occur and gas build-up can thus occur to eventually reach CO₂



79 supersaturation conditions, followed by a sudden gas burst.
80 In this study, we investigate the characteristics of lake stratification and overturning events at
81 Lake Albano through the results of 3D numerical model simulations, supported by
82 instrumental data collected from temperature sensors attached to drifters and buoys, used to
83 calibrate and validate the model.



84
85 **Figure 1:** Schematic illustration of the lake seasonal conditions with a typical winter
86 overturning and summer stratification (depth and horizontal extension of the lake are not in
87 scale).

88

89 **2. Modeling the volcanic Lake Albano**

90 In this study, the physics of the lake dynamics is investigated for the first time for Lake
91 Albano by a numerical model. It was not explored by previous works (Carapezza et al. 2008;
92 Chiodini et al. 2012; Rouwet et al. 2021) because the usual description of the lake behavior
93 was provided by analyzing vertical profiles of the physical-chemical properties along the
94 vertical profile at maximum lake depth. This 2D description may be adequate for a general
95 characterization of the lake conditions, but a 3D representation is essential for fully resolving
96 the lake dynamics and variations of physical-chemical characteristics in time and space.

97 The general ocean circulation numerical model SHYFEM (System of Hydrodynamic Finite
98 Element Modules) (Unglessier et al. 2004) is implemented for Lake Albano in order to (1)
99 reproduce the lake dynamics throughout the year, and (2) given its importance in hazard
100 evaluation, represent the volcanic lake system during the winter overturning.
101 The volcanic lake system is subjected to recurrent phases of recharging and emission of CO₂.
102 The yearly release of CO₂ depends on the vertical stratification, which is determined by the
103 lake surface-atmosphere heat fluxes. Thus, the implementation of a numerical model forced



104 by atmospheric reanalysis fields enables the representation of seasonal and interannual
105 cycles.

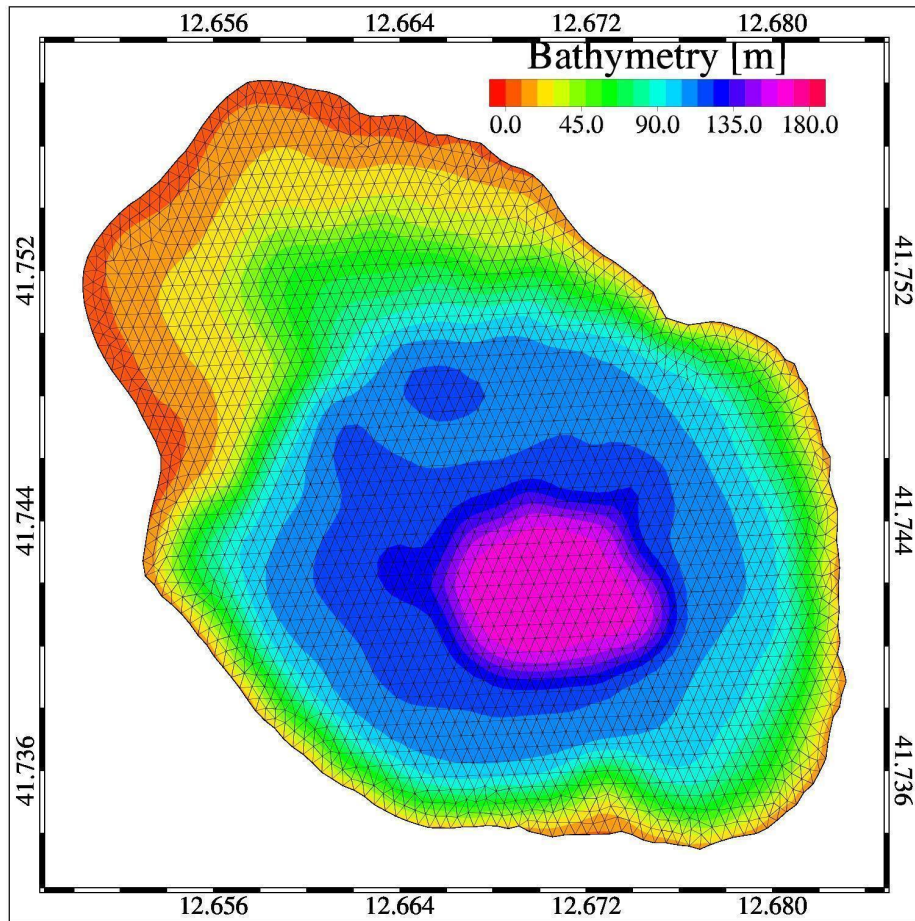
106 **2.1 System of HydrodYnamic Finite Element Modules (SHYFEM)**

107 A configuration of the SHYFEM model was implemented for Lake Albano (**Figure 2**).
108 SHYFEM is a framework of numerical models (SHYFEM, <http://www.ismar.cnr.it/shyfem>
109 and <https://github.com/georgu/shyfemcm-ismar>) to simulate the water movement and
110 temperature and salinity variables in an aquatic environment. It is a community model
111 developed by Italian and international institutes. SHYFEM consists of a finite element 3-D
112 hydrodynamic model, a transport and diffusion model and a radiation transfer model of heat at
113 the water surface. SHYFEM was previously successfully applied to many coastal environments
114 (Ferrarin and Umgiesser 2005; Ferrarin et al. 2010; Bellafiore et al. 2011; De Pascalis et al.
115 2011; Ferrarin et al. 2013, Umgiesser et al. 2014) and lakes (De Pascalis et al., 2009; Le Thi et
116 al. 2012). For more details of the model equations and their solution, please see Umgiesser et
117 al. (2004).

118 **2.2 Lake Albano model settings and parameterizations**

119 The lake bathymetry is derived from Anzidei et al. (2006; 2007; 2010), originally provided at
120 2 m of resolution. The model grid horizontal resolution ranges from 34 m to 66 m, due to the
121 varying size of the grid elements (**Figure 2**). The grid consists of 3016 nodes, 5831 elements,
122 and 89 vertical z levels, with thickness variable from 1 m (from the surface to the depth of 50
123 m) to 3 m (from 50 m to the maximum depth of 167 m). This horizontal and vertical
124 discretization appears adequate to satisfactorily resolve the major horizontal dynamical
125 structures and the vertical stratification of the lake.

126 No slip condition is set at the boundary/bottom (u and v velocity components equal 0). At the
127 boundary, water fluxes could be activated to account for sources such as groundwater
128 contributions. However, despite qualitative indications on the locations of inflow/outflow
129 (Mazza et al. 2015), the absence of data throughout the year prevents the inclusion of
130 groundwater flux values in the model used in the present study.



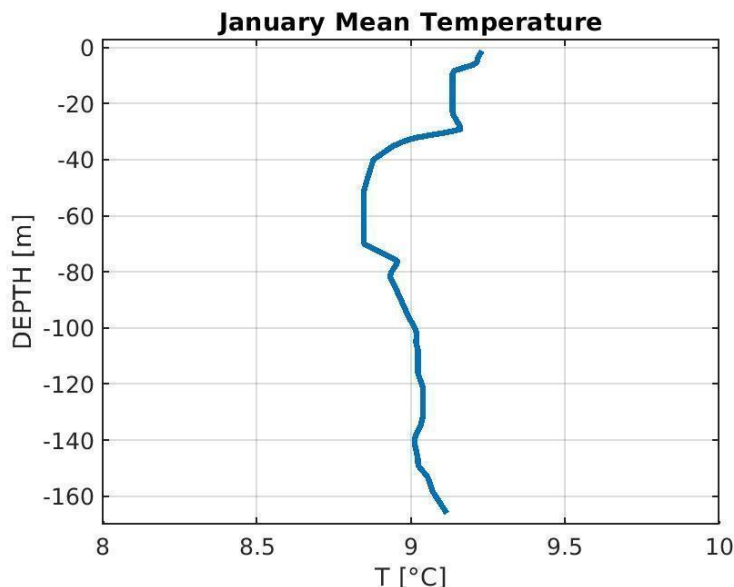
131
132 **Figure 2:** Model bathymetry of Lake Albano with the model mesh superimposed.
133

134 The model starts from rest. The initial conditions are based on homogeneous temperature (T)
135 and salinity (S) fields derived from averaging the vertical profiles of background observations
136 available from previous studies (Cioni et al. 2003; Carapezza et al. 2008; Ellwood et al.
137 2009). The temperature and salinity observed data were collected along the vertical profile of
138 the deepest part of Lake Albano. A set of monthly temperature measurements was available,
139 so the initial T field is based on the time-averaged observed values for the month used to start
140 the simulation, in this case January (Figure 3a). On the contrary, the paucity of salinity data
141 (main components are Na , K , Mg , Ca , HCO_3 , SO_4 , Cl), allowed only the setting of a mean
142 annual S field profile (Figure 3b). In order to construct the 3D initial conditions fields
143 required by the model, the temperature and salinity profiles are replicated across all the points
144 of the model grid.



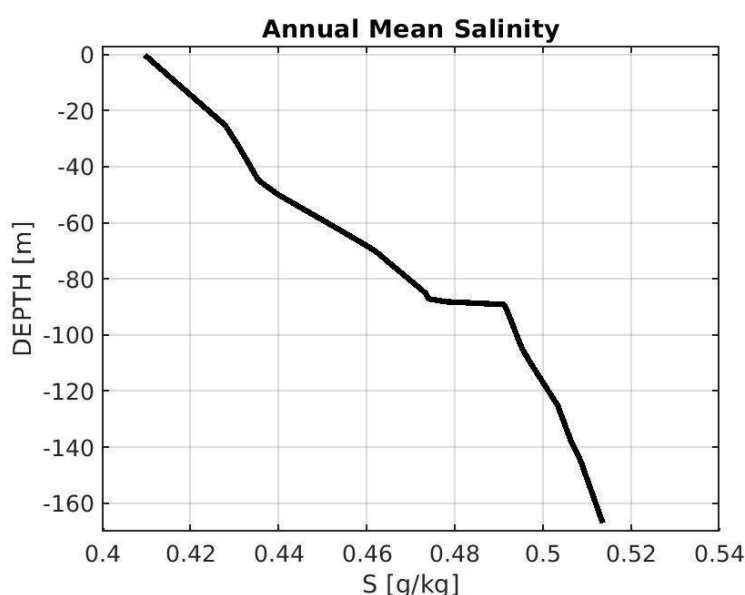
145

a)



146

b)



147

Figure 3: a) Initial Conditions for temperature (T) and b) salinity (S) fields derived from observations available in the deepest part of Lake Albano.

148

149

150 The atmospheric fields forcing used in the numerical model (10 m zonal and meridional wind
151 components, 2 m dew point temperature, mean sea level pressure, 2 m temperature, total
152 precipitation, total cloud cover, surface solar radiation downwards) are derived from the



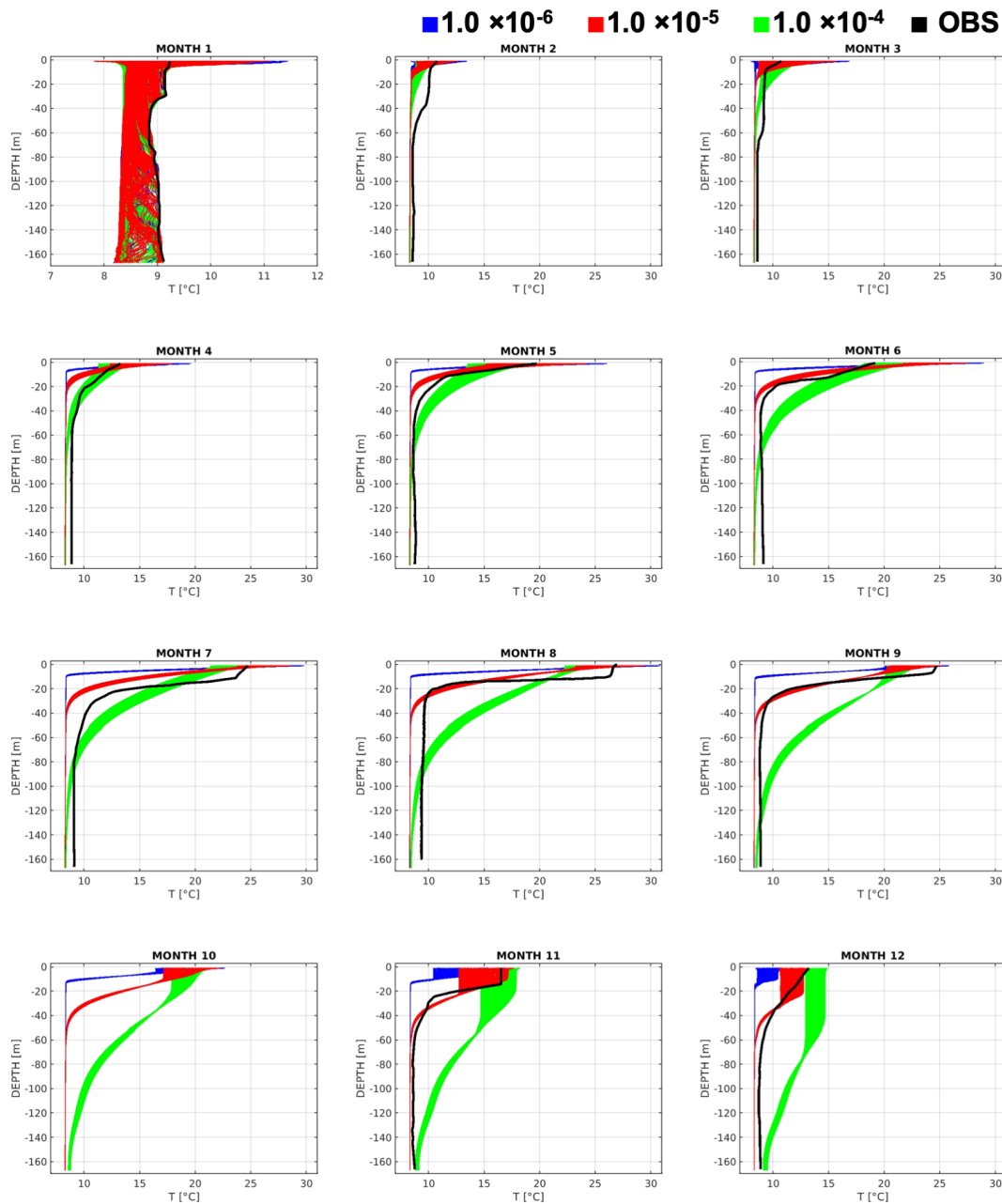
153 ERA5 reanalyses product (Hersbach et al. 2020; Bell et al. 2021), which has a 1/4-degree
154 horizontal resolution and an hourly temporal resolution.

155 In order to exclude bias and trends in the numerical solution due to atmospheric forcing, a set
156 of perpetual year experiments is performed. The simulations are forced by ERA5 reanalysis
157 fields averaged over the period 1979 - 2019 to build a climatological forcing data set.

158 Two numerical experiments were performed with the aim of
159 1) reproducing the seasonal thermocline according to the available observations, and
160 2) avoiding trends and biases that could cause deviations from the observed vertical
161 temperature profiles after several years, especially in the deepest levels.
162 In the case of the numerical experiment 1 the tested model parameter was the vertical
163 diffusivity, while in the case of the numerical experiment 2 the tested model parameters were
164 related to the air-water fluxes bulk formulas and were tested in absence of precipitation input.

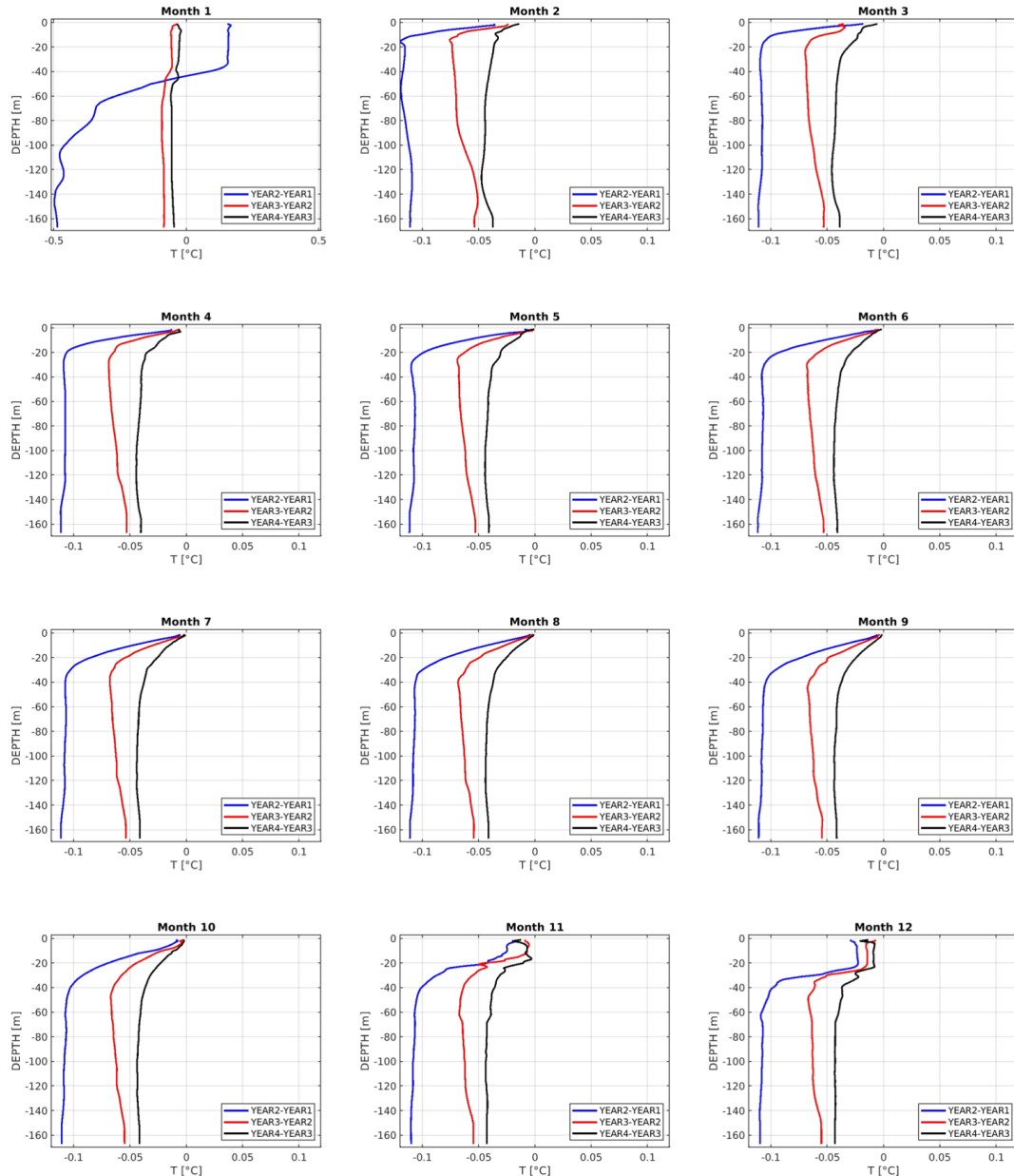
165 The results of the numerical experiments showed that the vertical diffusivity value which
166 optimizes the agreement between the modeled temperature profiles and the available
167 observations is 1.0×10^{-5} . This setting in the numerical experiment 1 maintains the thermocline
168 shallower than 40 m depth during the year ([Figure 4](#)).

169 The heat flux formulation that minimizes the temperature trends over the course of the
170 simulation is the one proposed by Large and Pond (1981), used also in Princeton Ocean Model
171 (POM). This setting in the numerical experiment 2 avoids trends and keeps the temperature
172 variation below 0.05 °C (well below the observed monthly mean variability) along the vertical
173 profiles. The interannual differences of the temperature profiles in the deepest part of the lake
174 are calculated month by month and are shown in [Figure 5](#).



175

176 **Figure 4:** Numerical experiment 1 for different vertical diffusivity values used to maintain the
 177 seasonal thermocline below 40 m depth.



178

179 **Figure 5:** Numerical experiment 2 for air-water fluxes bulk formulas as in the Princeton
180 Ocean Model used to reduce temperature deviation from observed data over time.

181

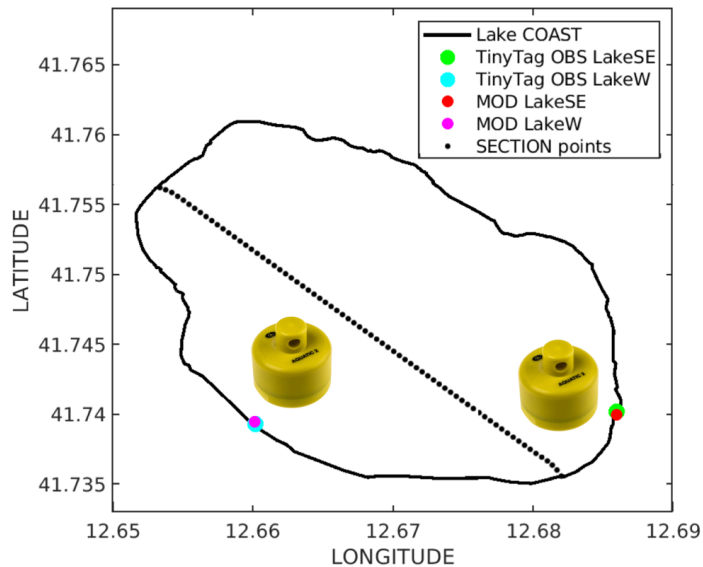
182 **3. Model validation and observations**



183 After the testing phase shown in the previous section, which was devoted to identifying the
184 optimal model setup, a numerical simulation over the period 1st January 2020 - 31st December
185 2023, was performed. To monitor the thermodynamic characteristics of the lake and support
186 the validation activities of the implemented numerical model, in the framework of the
187 MACMAP project (<https://progetti.ingv.it/it/progetti-dipartimentali/ambiente/macmap>) data
188 loggers at fixed locations (since May 2022) and drifters deployed into the waters of the lake
189 (August 2022 campaign) were used to collect temperature data and information on surface
190 circulation, respectively.

191 **3.1 Eulerian data**

192 Two temperature loggers (Tinytag Aquatic 2, Gemini TG-4100, resolution ± 0.01 °C) were
193 installed in May 2022 on the southeastern and western shores of the lake to continuously
194 record the surface water temperature. Measurements were collected every 30 minutes, stored
195 and retrieved during field campaigns ([Figure 6](#)).



196

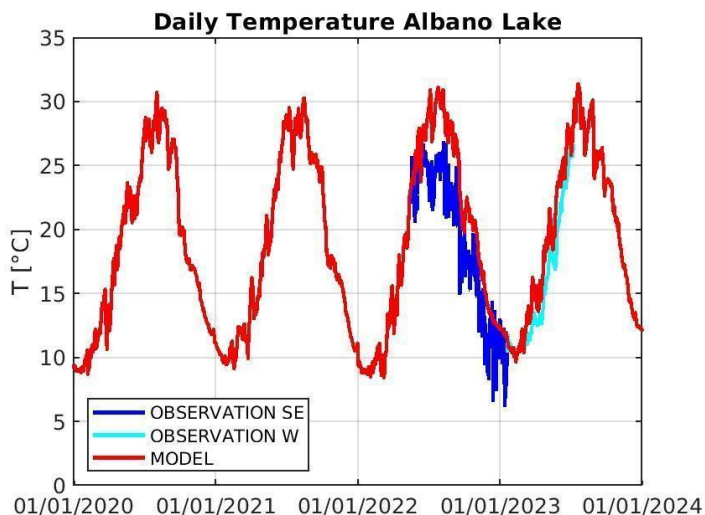
197 **Figure 6:** Locations of the installed temperature loggers (Tinytag Aquatic 2, Gemini
198 TG-4100, resolution ± 0.01 °C, [https://it.rs-](https://it.rs-online.com/web/p/datalogger/0283915?cm_mmc=IT-PLA-DS3A--google--CSS_IT_IT_PMAX_Catch+All_NEW---283915&matchtype=&&gclid=aw.ds&gad_source=1&gbraid=0AAAAADkeWNNt2RVFl68WQ111dWeSAEo9&gclid=CjwKCAiA5eC9BhAuEiwA3CKwQswZ0Q5C0R1ey9OHN6urIPP)
199 [online.com/web/p/datalogger/0283915?cm_mmc=IT-PLA-DS3A--google--CSS_IT_IT_PMAX_Catch+All_NEW---283915&matchtype=&&gclid=aw.ds&gad_source=1&gbraid=0AAAAADkeWNNt2RVFl68WQ111dWeSAEo9&gclid=CjwKCAiA5eC9BhAuEiwA3CKwQswZ0Q5C0R1ey9OHN6urIPP">online.com/web/p/datalogger/0283915?cm_mmc=IT-PLA-DS3A--google--CSS_IT_IT_PMAX_Catch+All_NEW---283915&matchtype=&&gclid=aw.ds&gad_source=1&gbraid=0AAAAADkeWNNt2RVFl68WQ111dWeSAEo9&gclid=CjwKCAiA5eC9BhAuEiwA3CKwQswZ0Q5C0R1ey9OHN6urIPP](https://it.rs-online.com/web/p/datalogger/0283915?cm_mmc=IT-PLA-DS3A--google--CSS_IT_IT_PMAX_Catch+All_NEW---283915&matchtype=&&gclid=aw.ds&gad_source=1&gbraid=0AAAAADkeWNNt2RVFl68WQ111dWeSAEo9&gclid=CjwKCAiA5eC9BhAuEiwA3CKwQswZ0Q5C0R1ey9OHN6urIPP)



203 [aN_9m92kM0DvESYGS9zfjw-5d6pNkXBoCf7QOAyD_BwE](#)) and the nearest model grid
204 points. In addition, the black dots indicate the section shown in Figures 10-13.

205

206 The recorded time series were used to assess the model's capability in reproducing the lake
207 temperature and its variability throughout the year. The average root mean square error
208 (RMSE) between modeled and observed temperature is slightly larger than 3 °C. However, in
209 the winter time the RMSE is reduced. In fact, in the temporal interval 01-Jan-2023 00:30:00-
210 31-Jan-2023 00:30:00 the RMSE is 2.12. The temperature seasonal variability is correctly
211 reproduced by the model, as confirmed by **Figure 7**, although an evident bias is present with
212 respect to the data recorded by the data logger installed on the southeastern shore of the lake
213 (blue curve in **Figure 7**). It is worth to note that the southeastern Tinytag data logger
214 probably moved and emerged from the lake waters in 2022, but it was not possible to
215 reconstruct the exact time window of this unplanned displacement.



216

217 **Figure 7:** Temperature recorded by the data loggers (blue and cyan curves indicate the SE
218 and W observations, respectively) and modeled temperature at the nearest locations where
219 the data loggers (Tinytags) were installed (red curve).

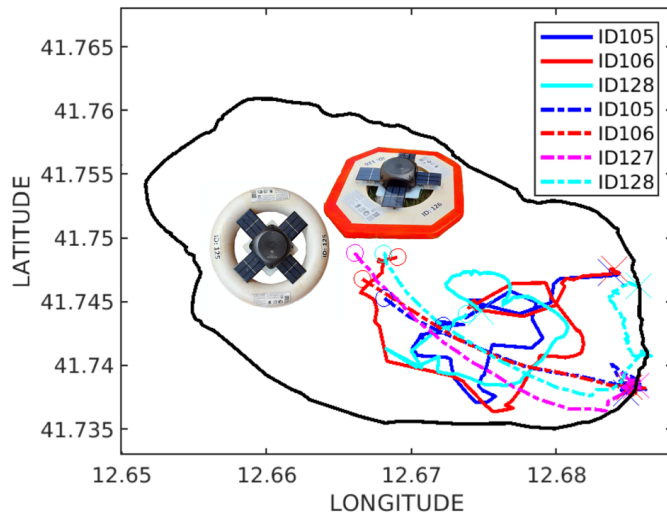
220

221 3.2 Lagrangian data

222 The lake's surface circulation was investigated using in-house assembled, low-cost drifters
223 originally employed to study the dynamics of litter of riverine origin (as described in Merlino
224 et al. 2023). The initial drifters (<http://carthe.org>, Novelli et al. 2017) were entirely
225 transformed for the purpose of this project. The innovative, reliable, robust, self-powered and
226 low cost "Marine Litter Trackers" (MLT) were developed in the framework of the ML-DAR



227 project (A multidisciplinary method to study the Marine Litter Dispersion from the Arno
228 River mouth: a study case to support citizen science, funded by INGV) and finally they were
229 re-adapted to be utilized as surface current trackers for this study. Two different kinds of
230 support were used: wooden tablets and floating supports. Some types of drifters were
231 equipped with cloth drogues that allow them to better follow the surface current and be less
232 affected by wind at the lake surface. Moreover, temperature sensors were installed on the
233 devices, in order to acquire surface water temperature data, in addition to tracking surface
234 currents.



235

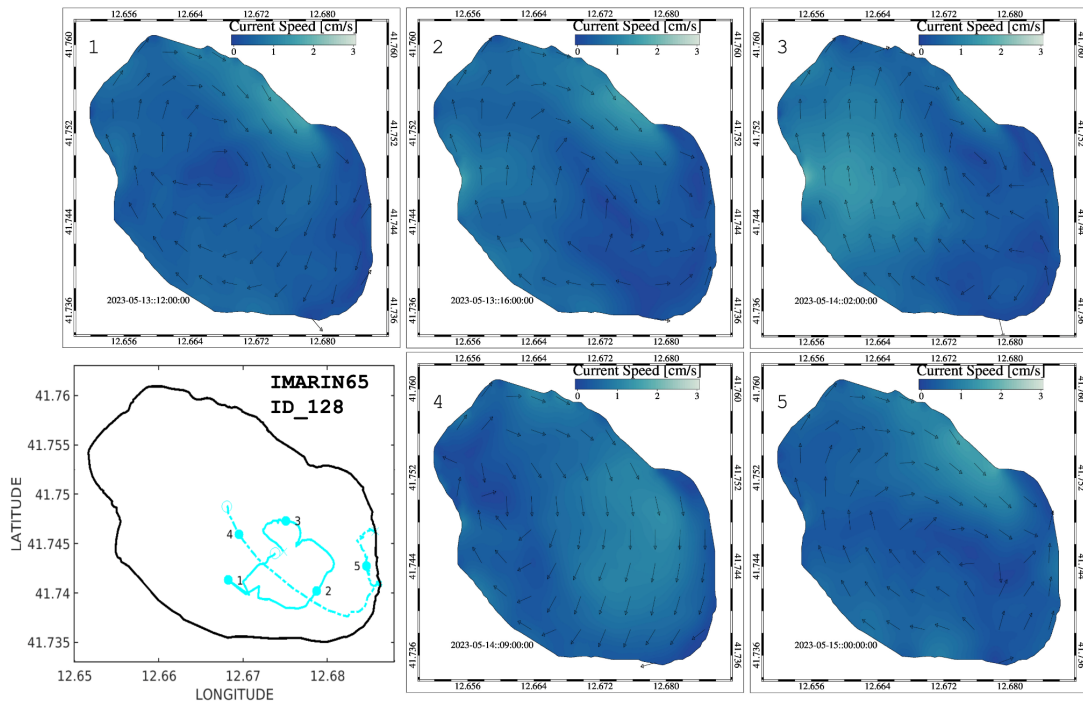
236 **Figure 8:** Images of the types of drifter deployed in Lake Albano and trajectories acquired by
237 the instruments (identified by the ID numbers) during the second survey (13-15 May 2023).
238 Solid lines indicate the trajectories of the drifters deployed on day 13th, dashed lines are the
239 trajectories of the same drifters deployed on day 14th. Picture of the drifters used, including
240 the modified CARTHEs, from which the battery packs and satellite antenna were removed,
241 replaced by the small central box with the consumer electronics of our mini drifters (SD card,
242 batteries, GPS antenna, GSM antenna), from the 4 photovoltaic cells in a halo, and to which
243 a temperature sensor was added (Merlino et al. 2023, DATA SET-repository: https://data-nautilus-h2020.eu/erddap/tabledap/mini_drifter.html).

245

246 The drifters were deployed in Lake Albano during two different surveys: a first one carried
247 out on 30th August and 1st September 2022 (mainly devoted to testing the drifters in a lake



248 environment) and a second one from 13th to 15th May 2023 (the acquired trajectories are
249 shown in [Figure 8](#)). A comparison was then performed between the trajectories recorded by
250 the drifters and the modeled surface currents for the three days of the second survey. A first
251 numerical experiment, forced by ERA5 atmospheric reanalyses, did not yield satisfactory
252 results, with drifter trajectories following a cyclonic pattern and modeled surface currents an
253 anticyclonic one in the same time frames (not shown). The reason for this discrepancy could
254 be due to the coarse, for our study area, spatial resolution of the ERA5 dataset (0.25 degree),
255 which probably limits the possibility to correctly reproduce the local wind regime. For this
256 reason, another numerical experiment was performed, retrieving the wind components from
257 an anemometer station located a few kilometers north-east of the lake
<https://www.wunderground.com/dashboard/pws/IMARIN65/graph/2023-05-15/2023-05-15/daily>. In this case a better agreement between the modeled surface currents and the drifter
259 trajectories is observed ([Figure 9](#)). Some discrepancies may be due to the course model
260 resolution which is not able to catch small features that drifters may be capable to follow.
261



262

263

264 **Figure 9:** Modeled surface currents on 13-15 May 2023 using the wind velocity field from the
265 anemometer IMARIN65 (model snapshots shown in the 1-5 panels) and trajectory of the
266 drifter ID_128 (first lower left panel).

267

268 **3.3 Winter Overturning**

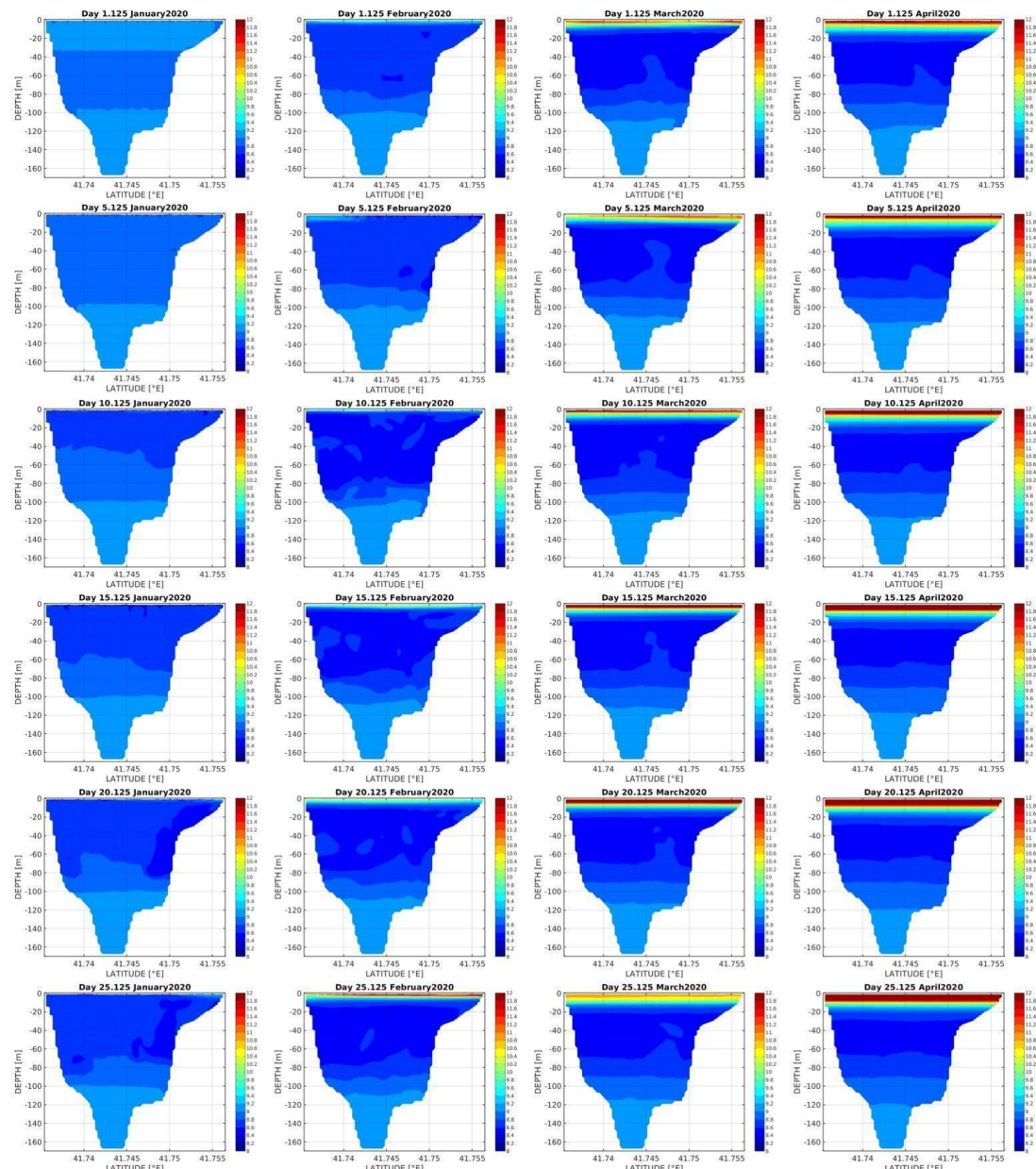


269 The model simulation covers a four-year period (01/01/2020 - 31/12/2023), with analyses
270 conducted on both a seasonal and interannual basis. **Figures 10-13** show temperature
271 longitudinal section for the winter period (January, February, and March, although some deep
272 vertical water temperature variations occur also in April). From the beginning of spring
273 (April) to the beginning of autumn (October), a remarkable vertical stratification is present
274 (**Figure 14** and **Supplementary Materials**), while from November a vertical mixing that
275 deepens progressively is observable from the temperature profiles.

276 Spatial variations in water density are basically driven by temperature, since salinity does not
277 show significant temporal and spatial variability (see **Figure 3**). The winter overturning is
278 strongly correlated with vertical temperature variations. Among the four years of simulation,
279 two years (2020 and 2022) exhibit winter overturning, which begins in the second decade of
280 January. Colder, and hence denser, water formation occurs in the northern shallow part of the
281 lake. Then, due to the lake's bathymetric configuration, denser waters move towards the deep
282 central part of the lake. Later, in February, cold water formation also occurs at the center of
283 Lake Albano (**Supplementary Materials**).

284 On some days in February and March it is possible to notice cold water patches moving from
285 the deeper layers towards the surface (**Supplementary Materials**).

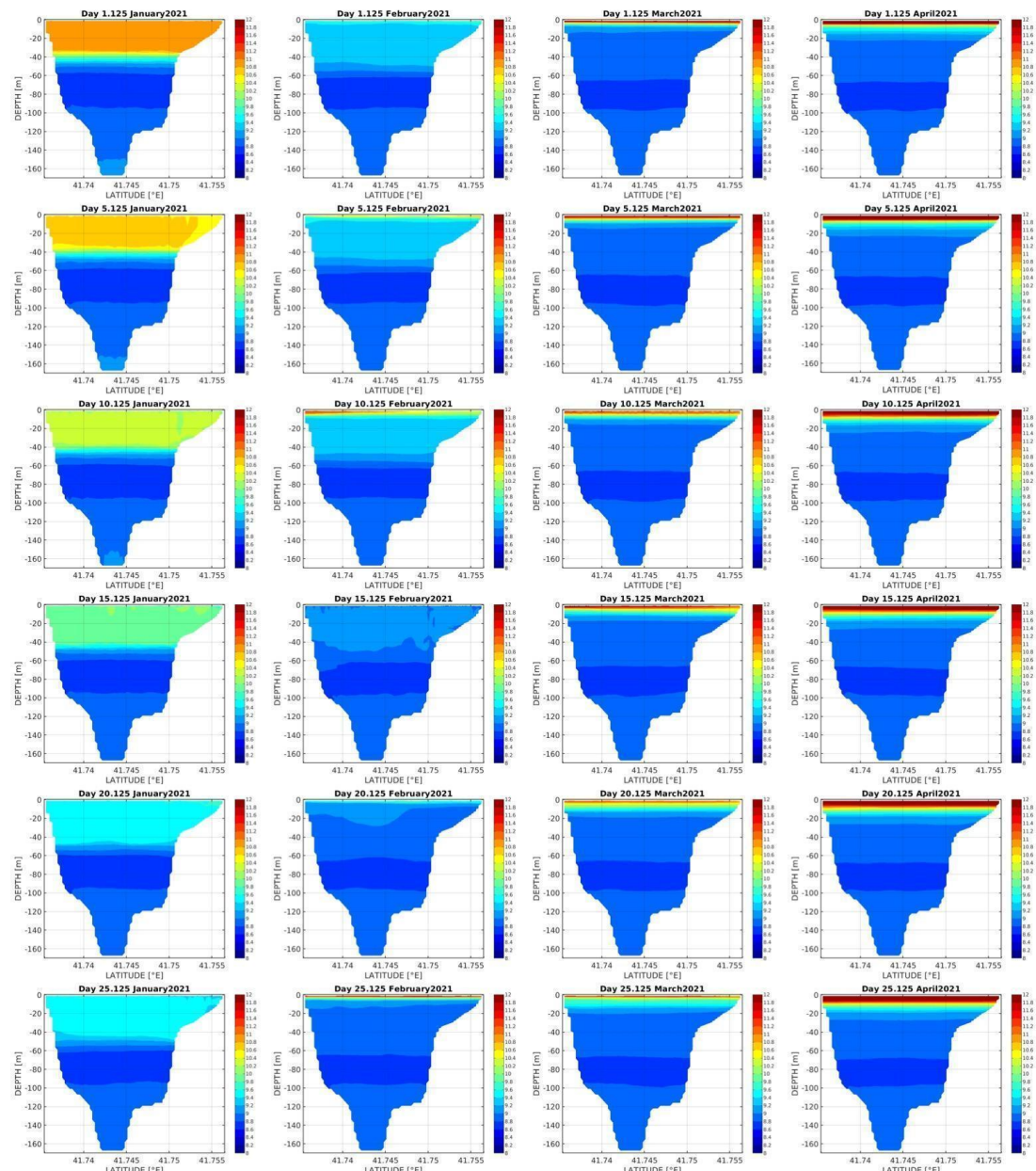
286 In some cases, intermediate layers (around 75-80 m depth, see video in Supplementary
287 material), exhibit colder temperatures compared to the layers directly above and below, until
288 the bottom, after the winter overturning. In these cases, vertical stability is still maintained,
289 because it is the total density that determines the stratification: despite being slightly warmer,
290 the deepest water layers are more saline, resulting in a higher total density at depth.



291

292 **Figure 10:** Modeled temperature T [$^{\circ}$ C] longitudinal sections in winter 2020.

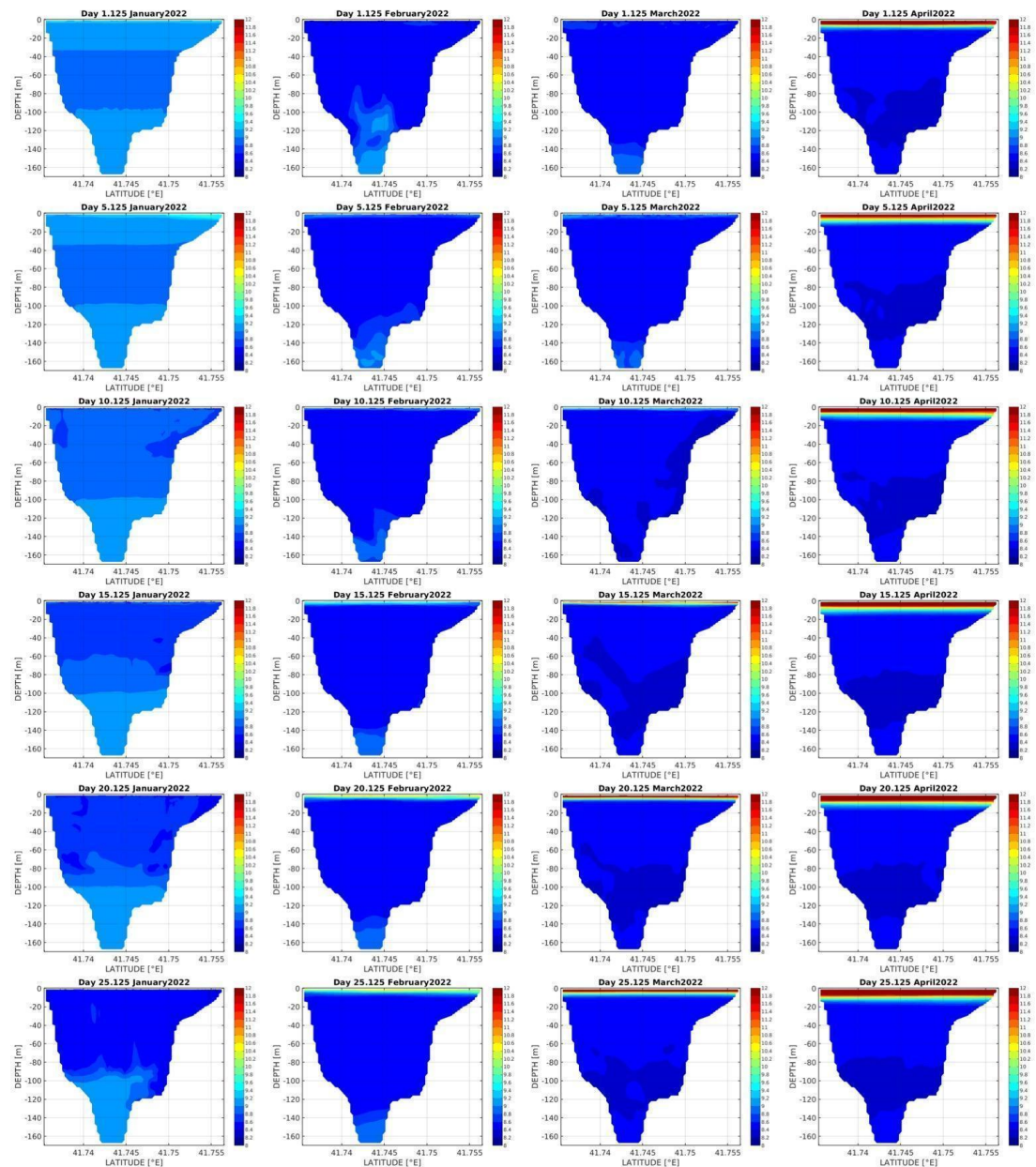
293



294

295 **Figure 11:** Modeled temperature T [$^{\circ}$ C] longitudinal sections in winter 2021.

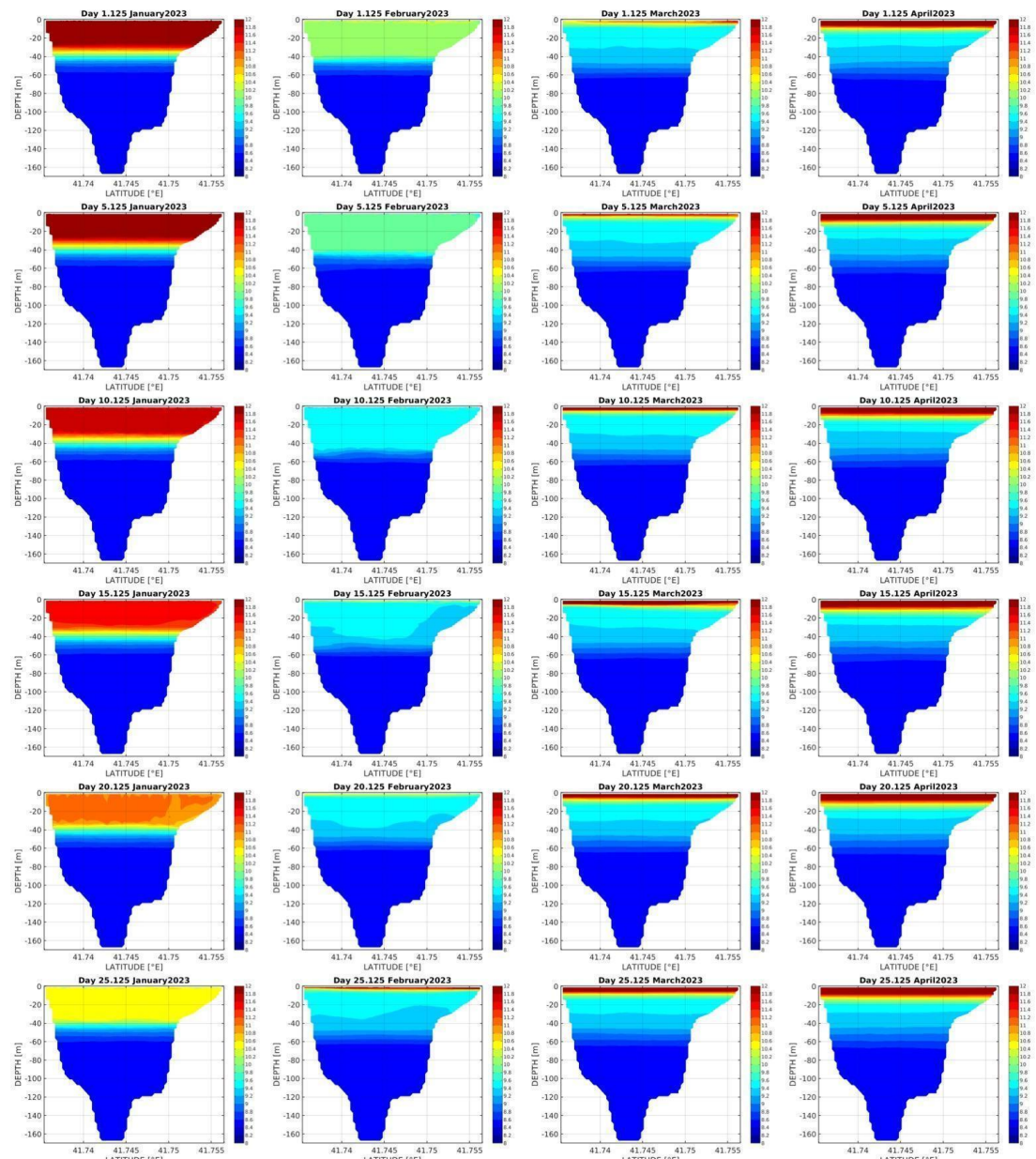
296



297

298 **Figure 12:** Modeled temperature T [$^{\circ}$ C] longitudinal sections in winter 2022.

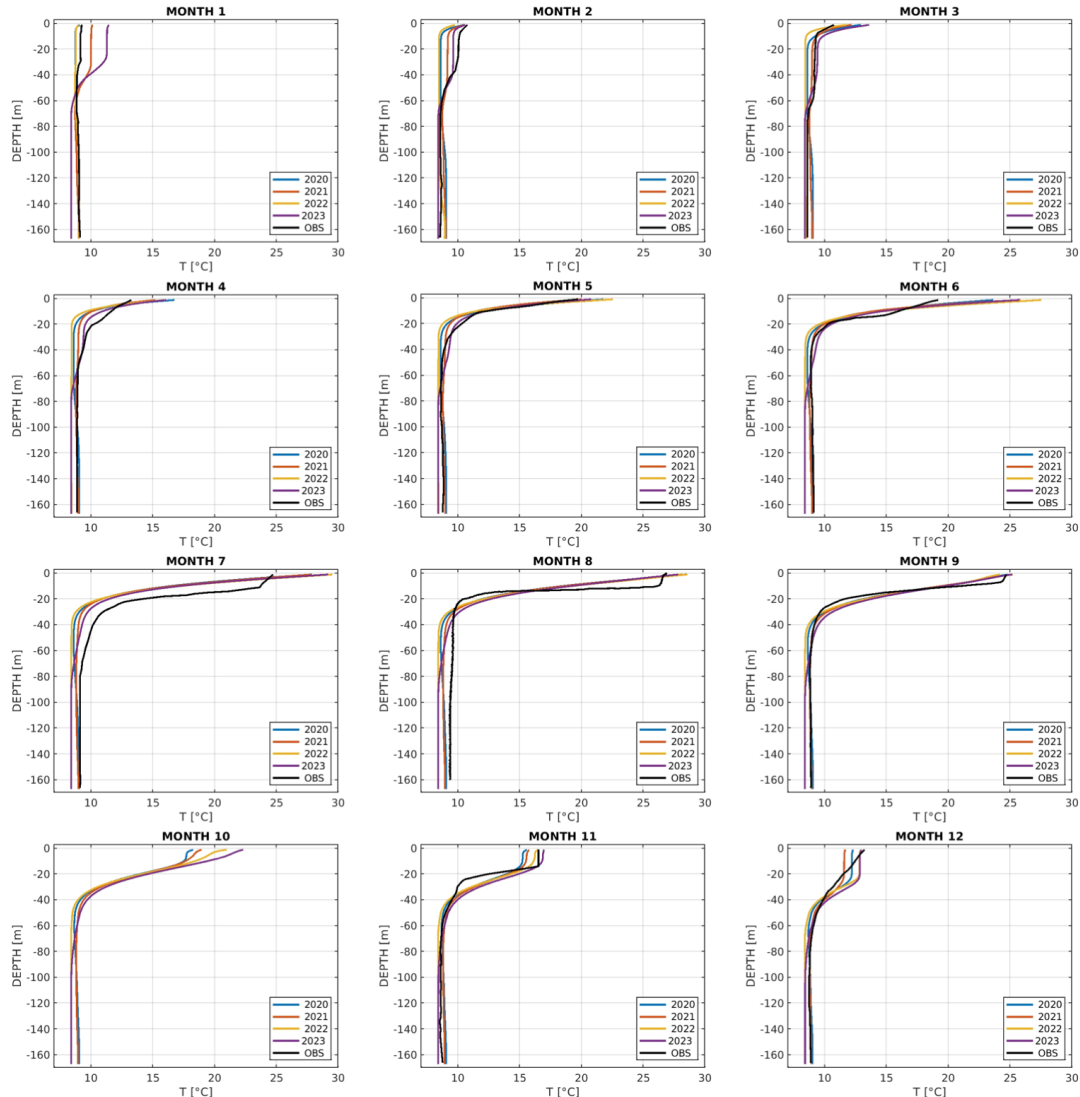
299



300

301 **Figure 13:** Modeled temperature longitudinal T [$^{\circ}$ C] sections in winter 2023.

302



303

304 **Figure 14:** Monthly averaged modeled and observed temperature profiles for the years 2020-
305 2023 (no observations available for October).

306

307 3.4 Overturning Index and Stability Index

308 In order to quantify the potential occurrence of overturning events, we computed the
309 overturning depth D_{overt}



310

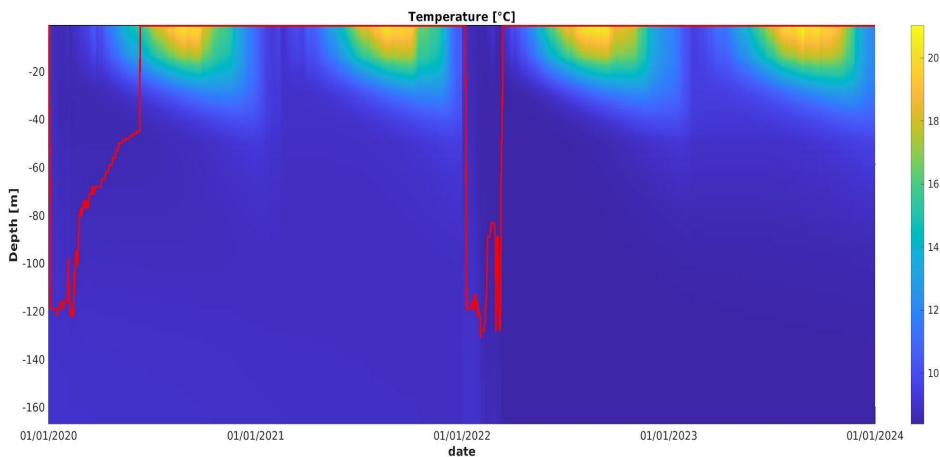
$$D_{overt} = \sum_{i=L_s}^{L_b} d_{level}(i) \cdot I_x(i)$$

311 where $L_s = 1 \text{ m}$ and $L_b = 167 \text{ m}$ are the surface and the bottom levels, d_{level} is the depth of
 312 each single level in the model, and I_x is the overturning index defined as following:

313 $I_x(i) = 0, \text{ if } T_{level}(i) \geq T_{mean}$
 314 $I_x(i) = 1, \text{ if } T_{level}(i) < T_{mean}$

315 with the mean temperature $T_{mean} = \text{mean}(T_{layerII}, T_{L_b})$. The $T_{layerII}$ and T_{L_b} are,
 316 respectively, the water temperature at the top of *layer II* (defined in Chiodini et al. 2012)
 317 which is located below 95 m, and the temperature of the deepest layers.

318 In other words, the index I_x compares the surface temperature with the temperature at
 319 maximum lake depth, so when surface temperatures are lower than deep temperatures,
 320 overturning conditions may be present. **Figure 15** shows the Howmoller diagram of the
 321 temperature profiles at the deepest point of the lake for the entire simulation period. As such,
 322 the levels involved in the overturning mechanism can extend below 100 m, reaching depths
 323 of up to 120 m, hence deeper than previously thought (Chiodini et al. 2012).



324

325 **Figure 15:** Howmoller diagram of the temperature profiles at the deepest point of the lake
 326 and I_x index values (red line).

327

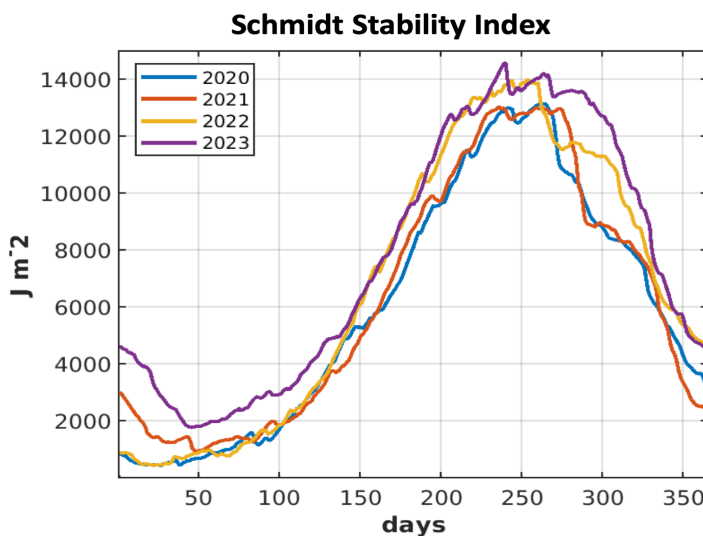
328 By comparing temperature values at different lake depths, the results show that temperatures
 329 at 1 m (T1) are lower than those at depths below 95 m for 35 days in the 2020 winter and 29
 330 days in the 2022 winter at the point of maximum lake depth. This time window indicates
 331 when and for how long the surface water is colder than the deeper layers, making it able to
 332 sink and trigger lake overturning. In 2021 and 2023, by contrast, surface temperatures (T1)
 333 never fall below the temperature at 40 m.



334 For completeness, the Schmidt stability index (Schmidt, 1928) was computed to characterize
335 the stability of a stratified water column. It is a measure of the energy required to completely
336 mix a stratified lake with an arbitrary vertical density distribution, taking into account the
337 volume of the lake basin (Kirillin and Shatwell, 2016). It represents the work required for its
338 mechanical mixing without heat exchange with the environment per unit area (Smirnov et al.,
339 2024). The Schmidt stability index St is expressed by

340
$$St = g A_0 \int_0^{Hmax} (z - z_v) \rho_z A_z dz$$

341 where g is acceleration of gravity, ρ_z is water density at depth z , A_0 is lake surface area, A_z
342 is lake area under the isobath z , $Hmax$ is maximal lake depth, z_v is the depth to the center of
343 lake volume, calculated as: $z_v = \frac{1}{V} \int_0^{Hmax} (z - z_v) A_z dz$, V being the lake volume. The
344 adequate assessment of Schmidt stability requires eliminating variations in temperature
345 profiles, so model daily averaged temperature values are used in the analysis. The computed
346 St values (shown in **Figure 16**) fall within a range consistent with recent studies on the
347 physical limnology of Italian lakes (Ambrosetti et al. 2002) and confirm that the energy
348 required to vertically mix the water column is lower for 2020 and 2022.



349

350 **Figure 16:** Schmidt stability index computed for the years 2020-2023.

351

352 **4. Discussion and Conclusions**

353 The 3D SHYFEM model was implemented to simulate the physical dynamics of the volcanic



354 Lake Albano. A numerical experiment was performed from 01/01/2020 to 31/12/2023 for
355 investigating seasonal and interannual lake variability.

356 Major findings of this study are:

357 - the winter overturning mechanism is driven by atmospheric forcing and does not occur
358 every year, but only when the surface thermal conditions are suitable. Atmospheric
359 forcing causes the cooling of the lake surface and triggers the overturning, typically in
360 January. Over the four years simulation, winter overturning occurred twice (in 2020
361 and 2022), starting after mid-January and lasting for a few weeks, before the spring-
362 summer stratification resumes until the following winter. In both 2021 and 2023, the
363 stratification starts very early and surface cooling results insufficient for the lake to
364 overturn.

365 - cold water formation begins in the shallow northern part of the lake and spreads
366 southeastward toward the deeper lake levels. When surface cooling is intense in the
367 middle of the winter, the cold water sinks down to the lake bottom at 167 m;

368 - the winter overturning in 2020 and 2022 involves the rise of water layers from depths
369 greater than 95 m, with cold water patches moving towards the surface. Given that (i)
370 CO₂ is more soluble in cold water, (ii) deep water layers are enriched in CO₂, and (iii)
371 no bubble degassing is observed during winter overturn, this upward movement of cold
372 CO₂-enriched deep water may be the physical mechanism behind CO₂ release during
373 winter overturning, in agreement with previous degassing models and trends
374 (Carapezza et al. 2008; Chiodini et al. 2012; Rouwet et al. 2021);

375 - after the winter overturning, surface temperatures follow the seasonal variations of the
376 atmospheric temperature. Strong thermal stratification of the lake persists above the
377 thermocline during the warmest seasons. Below 40-50 m, the temperature usually
378 remains between 8.0-9.5 °C throughout the year, as confirmed by the available
379 observations.

380 Although the spatial resolution of ERA5 atmospheric fields may be considered too coarse for
381 the lake area, the air-lake heat fluxes in this region are considered suitable for investigating the
382 winter overturning mechanism. In fact, the modeled surface temperature follows the observed
383 seasonal temperature variations. To better reproduce surface circulation patterns, local wind
384 forcing would be required, in order to introduce finer-scale variability.

385 Another limitation is the lack of groundwater data. Even if the SHYFEM model can simulate
386 water fluxes at the lake boundaries, the lack of this data prevents the inclusion of interactions
387 between groundwater and lake water, as well as processes related to further temperature
388 variations. Including such processes would require a multi-scale approach that combines
389 multiple measurement methods, considerable constraints and uncertainties, and the estimation
390 of the fluxes between groundwater and lake water at different spatial and temporal scales.

391 Increasing surface water temperatures due to global warming could enhance vertical water
392 stratification and potentially inhibit or reduce the frequency of the overturning process. As a



393 consequence, in the case of less frequent winter overturning, CO₂ accumulated over the years
394 (following seismically induced recharge, Chiodini et al. 2012), may increase limnic gas hazard
395 for Lake Albano when overturn does occur. In the extreme case where Lake Albano ceases to
396 overturn due to ongoing atmospheric warming, CO₂ could remain stored in the deep lake layers
397 until supersaturation conditions will be reached, potentially triggering a “Nyos-type” gas burst.
398 So, the numerical model implemented in this study, tracking atmospheric and surface water
399 temperatures at Lake Albano, could provide a basic framework for monitoring future degassing
400 dynamics. Moreover, simulations of Lake Albano could reproduce the past dynamical
401 evolution of the lake and may also reconstruct its behaviour in relation to both the seismic
402 swarms in the Colli Albano area in 1987-1990 and the decline of the lake water surface levels
403 due to anthropic activities over the last decades, which is expected to continue in the coming
404 years. Concerning the fluctuation of the lake level, a continuous lowering of its level started in
405 1970 (Anzidei et al. 2010) with a continuous acceleration during the following decades (Capelli
406 et al. 2000; Capelli and Mazza 2005; Riguzzi et al. 2008; Mazza and Capelli 2010). The lake
407 level remained about stable between 1940 and 1960. Then, a lake level fall occurred at a mean
408 rate of 8.8 cm/yr in 1960-2005 and then at 20 cm/yr in 1990-1997 (Anzidei and Esposito 2010).
409 The cause of the lake level fall has been largely attributed to the excessive ground water
410 withdrawal (Capelli and Mazza 2005) or in connection with shallow seismicity (Bianchi et al.
411 2008; Chiarabba et al. 2010) and ground uplift (Amato and Chiarabba 1995; Riguzzi et al.
412 2009; Anzidei et al. 2010). The hypocenters of the latest earthquakes occurred in 1987-1990 in
413 this area were aligned along a NW-SE striking structure across the Lake Albano and the other
414 craters of the Colli Albano volcano (Amato et al. 1994, Bianchi et al. 2008). It is worth noting,
415 that during this seismic period, a significant lake level drop occurred in 1990. This phenomenon
416 has been addressed to an increased permeability of the lake basin in response of endogenous
417 processes.

418 Finally, despite the lake level changes, the model implemented could be applied to other
419 volcanic lakes to investigate their dynamics and associated physical and chemical processes.

420

421 **Author Contribution**

422 AG conceived the study, implemented the model, computed the simulations and wrote the
423 draft manuscript; DD prepared the forcing and supported the model implementation for
424 parallel computing; GU supported the model implementation; MA provided the Albano
425 bathymetry; DR installed the tinytags and prepared the Eulerian data; MB, SM, MP, ML and
426 FM deployed and prepared the drifters providing the lagrangian data; GT prepared the wind
427 velocity field from the anemometer. All authors worked collaboratively to interpret the data
428 and finalized the writing of the manuscript for publication.

429

430 **Competing Interests**

431 The authors declare that they have no conflict of interest.

432



433 **Acknowledgments**

434 We thank Claudia Fratianni for supporting the procedure to include the “Supplementary
435 Materials” in the ERDDAP system for the easier access to scientific data.

436 This study has been developed in the framework of the MACMAP project funded by Istituto
437 Nazionale di Geofisica e Vulcanologia (Environment Department). Bathymetric Surveys
438 were performed in 2007 under the Colli Albani Project V-3 funded by the Italian
439 Dipartimento della Protezione Civile.

440

441 **Supplementary Materials**

442 Additional materials are movies of the simulation of the January, February, March and April
443 months for the 2020-2023 years and they can be downloaded at the following link
444 http://oceano.bo.ingv.it/erddap/files/albano_lake_model_video/.
445

446 **References**

447 Amato, A. & Chiarabba, C. (1995) Recent uplift of the Alban Hills Volcano (Italy): evidence
448 for magmatic inflation? *Geophysical Research Letters*, 22, 1985 – 1988.

449 Amato, A., Chiarabba, C., Cocco, M., Di Bona, M. & Selvaggi, G. (1994) The 1989 – 1990
450 seismic swarm in the Alban Hills volcanic area, central Italy. *Journal of Volcanology and*
451 *Geothermal Research*, 61, 225–237.

452 Ambrosetti, Walter & Barbanti, Luigi. (2002). Physical limnology of Italian lakes. 2.
453 Relationships between morphometric parameters, stability and Birgean work. *J. Limnol.* 61.
454 159-167. 10.4081/jlimnol.2002.159.

455 Anzidei M. & A. Esposito (2010) Lake Albano: bathymetry and level changes, From:
456 Funiciello, R. & Giordano, G. (eds) *The Colli Albani Volcano*. Special Publications of
457 IAVCEI, 3, 229–244. Geological Society, London. 1750-8207/10/\$15.00 # IAVCEI 2010.

458 Anzidei, M., A. Esposito, and F. De Giosa (2006). The dark side of the Albano crater lake.
459 *Annals of Geophysics*, 49, 1275-1287.

460 Anzidei M., M. L. Carapezza, A. Esposito, G. Giordano, M. Lelli, L. Tarchini (2008) The
461 Albano Maar Lake high resolution bathymetry and dissolved CO₂ budget (Colli Albani
462 volcano, Italy): Constraints to hazard evaluation, *Journal of Volcanology and Geothermal*
463 *Research* 171 258–268

464 Anzidei M, Esposito A. Lake Albano (2010). Lake Albano: bathymetry and level changes.
465 Special Publications of IAVCEI The Colli Albani Volcano. Editor(s) R. Funiciello; G.
466 Giordano. Geological Society of London, Vol.3. <https://doi.org/10.1144/IAVCEI003.12>

467 Anzidei, M., Riguzzi, F., Stramondo, S. (2010). Current geodetic deformation of the Colli
468 Albani volcano: a review. in Funiciello, R. & Giordano, G. (eds) *The Colli Albani Volcano*.
469 Special Publications of IAVCEI, 3, 299–310. Geological Society, London. 1750-
470 8207/10/\$15.00 # IAVCEI 2010



471 Bellafiore, D. and G. Umgiesser (2010). Hydrodynamic coastal processes in the North
472 Adriatic investigated with a 3D finite element model. *Ocean Dynamics*, Vol. 60 (2), 255-273.
473 DOI:10.1007/s10236-009-0254-x

474 Bianchi, I., Piana Agostinetti, N., De Gori, P. & Chiarabba, C. (2008) Deep structure of the
475 Colli Albani volcanic district (central Italy) from receiver functions analysis. *Journal
476 Geophysical Research*, 113, B09313, doi: 10.1029/2007JB005548.

477 Carapezza M.L., M. Lelli, L. Tarchini (2008) *Geochemistry Of The Albano And Nemi Crater
478 Lakes In The Volcanic District Of Alban Hills (Rome, Italy)*, *Journal Of Volcanology And
479 Geothermal Research*, 178, 297-304

480 Capelli, G. & Mazza, R. (2005) Water criticality in the Colli Albani (Rome, Italy). *Giornale di
481 Geologia. Applicata*, 1, 261 – 271, doi: 10.1474/GGA.2005- 01.0-26.0026.

482 Capelli G., Mazza R., Giordano G., Cecili A., De Rita D., Salvati D. (2000): The Colli Albani
483 Volcano (Rome, Italy): equilibrium breakdown of a hydrogeological units as a results of
484 unplanned and uncounted over exploitation. *Hydrogeological*, 4, 63-70

485 Cioni R., M. Guidi, B. Raco, L. Marini, B. Gambardella (2003) Water chemistry of Lake
486 Albano (Italy), *Journal of Volcanology and Geothermal Research*, 120, 179-195

487 Chiodini, G., Cioni, R., Guidi, M., Magro, G., Marini, L., Raco, B., (2000) Gas chemistry of
488 the Lake Piccolo of Monticchio, Mt. Vulture, in December 1996. *Acta Vulcanol.* 12, 139-
489 142.

490 Chiodini G, Cardellini C, Amato A, Boschi E, Caliro S, Frondini F, Ventura G (2004) Carbon
491 dioxide Earth degassing and seismogenesis in central and southern Italy. *Geophys Res Lett*
492 31(7). doi:L0761510.1029/2004GL019480

493 Chiodini, G., Tassi, F., Caliro, S., Chiarabba, C., Vaselli, O., Rouwet, D.,(2012). Time-
494 dependent CO₂ variations in Lake Albano associated with seismic activity. *Bull. Volcanol.*
495 74, 861-871. <https://link.springer.com/article/10.1007/s00445-011-0573-x>

496 Dagestad, K.-F., Röhrs, J., Breivik, Ø., and Ådlandsvik, B. (2018) OpenDrift v1.0: a generic
497 framework for trajectory modelling, *Geosci. Model Dev.*, 11, 1405–1420,
498 <https://doi.org/10.5194/gmd-11-1405-2018>

499 De Rita, D., Funiciello, R., Pantosti , D. (1987). Dynamics and evolution of the Albano crater,
500 south of Roma, Proceeding. IAVCEI International. Conference, Kagoshima, 502-505.

501 De Rita, D., Funiciello, R., Parotto, M. (1988). *Carta Geologica del Complesso vulcanico dei
502 Colli Albani* (Geological map of the Colli Albani volcanic complex), scale 1:50,000, Consiglio
503 Nazionale delle Ricerche.

504 Drakopoulos P. G. and A. Lascaratos (1999). Modelling the Mediterranean Sea: climatological
505 forcing *J. Mar. Sys.* 20 157-173

506 Ellwood N.T.W. , Patrizia Albertano, Rosa Galvez, Renato Funiciello, Rosario Mosello (2009)
507 *Water Chemistry And Trophic Evaluation Of Lake Albano (Central Italy): A Four Year Water
508 Monitoring Study*, *J. Limnol.*, 68(2), 288-303



509 Ferrarin, C. and G. Umgiesser (2005). Hydrodynamic modeling of a coastal lagoon: The
510 Cabras lagoon in Sardinia, Italy. *Ecological Modelling*, Vol. 188, 340-357.
511 DOI:10.1016/j.ecolmodel.2005.01.061

512 Ferrarin, C., G. Umgiesser, M. Bajo, D. Bellafiore, F. De Pascalis, M. Ghezzo, G. Mattassi
513 and I. Scroccaro (2010). Hydraulic zonation of the lagoons of Marano and Grado, Italy. A
514 modelling approach. *Estuarine, Coastal and Shelf Science*, Vol. 87 (4), 561-572.
515 DOI:10.1016/j.ecss.2010.02.012

516 Ferrarin, C., Bergamasco, A., Umgiesser, G. and Cucco, A. (2013). Hydrodynamics and
517 spatial zonation of the Capo Peloro coastal system (Sicily) through 3-D numerical modelling.
518 *Journal of Marine Systems*, Vol. 117-118, 96-107. DOI:10.1016/j.jmarsys.2013.02.005

519 Freda, C., Gaeta, M., Karner, D., Marra, F., Renne, P.R., Taddeucci, J., Scarlato, P.,
520 Christensen, J. N., Dallai, L. (2006). Eruptive history and petrologic evolution of the Albano
521 multiple maar (Alban Hills, Central Italy). *Bulletin of Volcanology*, 68, 6, 567-591.

522 Funiciello R, Giordano G, De Rita D (2003) The Albano maar lake (Colli Albani Volcano,
523 Italy): recent volcanic activity and evidence of pre-Roman Age catastrophic lahar events.
524 *Journal of Volcanology and Geothermal Research* 123: 43-61

525 Giordano, G. The CARG Team (2010). Stratigraphy and volcano-tectonic structures of the
526 Colli Albani volcanic field. In Funiciello, R. & Giordano, G. (eds) *The Colli Albani Volcano*.
527 Special Publication of IAVCEI, 3. The Geological Society, London, 000-000

528 Kanari S.I. (1989). *An Inference On The Process Of Gas Outburst From Lake Nyos, Cameroon*,
529 *Journal Of Volcanology And Geothermal Research*, 39, 135-149

530 Kirillin, G. , T. Shatwell (2016). *Generalized scaling of seasonal thermal stratification in*
531 *lakes*, *Earth-Science Reviews*, 161, 179-190, https://doi.org/10.1016/j.earscirev.2016.08.008.

532 G. W. Kling, M.L. Tuttle, W. C. Evans (1989) *The Evolution Of Thermal Structure And Water*
533 *Chemistry In Lake Nyos*, *Journal Of Volcanology And Geothermal Research*, 39, 151-165

534 G.W. Kling, W.C. Evans, G.Z. Tanyileke (2015). *The Comparative Limnology Of Lakes Nyos*
535 *And Monoun, Cameroon*, D. Rouwet Et Al. (Eds.), *Volcanic Lakes, Advances In Volcanology*,
536 Springer-verlag Berlin Heidelberg

537 M. Kusakabe (2017). *Lakes Nyos And Monoun Gas Disasters (Cameroon)—limnic Eruptions*
538 *Caused By Excessive Accumulation Of Magmatic CO₂ In Crater Lakes*, *Geochem. Monogr.*
539 Ser. 1: 1-50

540 Le Thi, Anh Dao, De Pascalis, F., Umgiesser, G. and Wildi, W. (2012). *Structure thermique*
541 *et courantologie du Léman (Thermal structure and circulation patterns of Lake Geneva)*.
542 *Archives des Sciences*, vol. 65, p. 65-80. ISSN: 1661-464X

543 Marra, F., Freda, C., Scarlato, P., Taddeucci, J., Karner, D.B., Renne, P.R., Gaeta, M.,
544 Palladino, D.M., Trigila, R., Cavarretta, G. (2003). Post-caldera activity in the Albani Hills
545 volcanic district (Italy): 40Ar/39Ar geochronology and insights into magma evolution.
546 *Bulletin of Volcanology*, 65, 227-247, doi: 10.1007/s00445-002-0255-9.



547 Mazza, R. & Capelli, G. (2010) Hydrogeology of the Colli Albani unit. In: Funiciello, R. &
548 Giordano, G. (eds) The Colli Albani Volcano. Geological Society, London, Special
549 Publications of IAVCEI, 3, 189–213.

550 Mazza R. , S. Taviani, G. Capelli, A.A. De Benedetti, and G. Giordano D. (2015) Quantitative
551 Hydrogeology of Volcanic Lakes: Examples from the Central Italy Volcanic Lake District pp
552 355-377 in Rouwet et al. (eds.), Volcanic Lakes, Advances in Volcanology, DOI 10.1007/978-
553 3-642-36833-2_16, Springer-Verlag Berlin Heidelberg

554 Merlini S, Locritani M, Guarneri A, Delrossi D, Bianucci M, Paterni M. (2023). Marine Litter
555 Tracking System: A Case Study with Open-Source Technology and a Citizen Science-Based
556 Approach. *Sensors*. 23(2):935. <https://doi.org/10.3390/s23020935>

557 Novelli G., C. M. Guigand, C. Cousin, E. H. Ryan, N. J.M. Laxague, H. Dai, B. K. Haus, and
558 T. M. Özgökmen (2017). A biodegradable surface drifter for ocean sampling on a massive
559 scale. *Journal of Atmospheric and Oceanic Technology*, 34, no. 11 : 2509-2532,
560 <https://journals.ametsoc.org/view/journals/atot/34/11/jtech-d-17-0055.1.xml>

561 Riguzzi, F., Pietrantonio, G., Devoti, R., Atzori, S. & Anzidei, M. (2009) Volcanic unrest of
562 the Colli Albani (central Italy) detected by GPS monitoring test. *Physics of the Earth and*
563 *Planetary Interiors*, 177, 79–87, doi: 10.1016/j.pepi.2009.07.012.

564 Rouwet, D., Chiodini, G., Ciuccarelli, C., Comastri, A., Costa, A., (2019). Lago Albano, the
565 “anti-Nyos-type” lake: The past as a key for the future. *J. Afric. Earth Sci.*,
566 <https://doi.org/10.1016/j.jafrearsci.2018.09.019>

567 Rouwet D., G. Tamburello, G. Chiodini, G. Pecoraino, M. Procesi, T. Ricci, S. Venturi, A.
568 Santi, J. Cabassi, O. Vaselli, F. Tassi & A. Costa (2021). New insights into the degassing
569 dynamics of Lago Albano (Colli Albani volcano, Rome, Italy) during the last three decades
570 (1989-2019) *Ital. J. Geosci.*, Vol. 140, No. 1. (<https://doi.org/10.3301/IJG.2020.19>)

571 Schmidt, W. (1928). Über die Temperatur- und Stabilitätsverhältnisse von Seen. *Geografiska*
572 *Annaler*, 10: 145-177.

573 Smirnov, S.I., Zdorovennov, R.E., Efremova, T.V. *et al.* (2024). Parameters of Water
574 Column Stability in a Small Polymictic Lake in Years of Different Weather Conditions.
575 *Water Resour* **51**, 299–313 <https://doi.org/10.1134/S0097807824700817>

576 Trigila, R. (ED) (1995). The volcano of the Alban Hills. Tipografia SGS, Rome, 283 pages.

577 Villa, I.M., Calanchi, N., Dinelli, E., Lucchini, F., (1999). Age and evolution of the Albano
578 crater lake (Roman Volcanic Province). *Acta Vulcanologica*, 11, 305-310.

579 Umgieser Georg, D. M. Canu, A. Cucco, C. Solidoro (2004). A finite element model for the
580 Venice Lagoon. Development, set up, calibration and validation, *Journal of Marine Systems*
581 51, 123– 145 doi:10.1016/j.jmarsys.2004.05.009

582 Umgieser, G., Ferrarin, C., Cucco, A., De Pascalis, F., Bellafiore, D., Ghezzo, M., & Bajo,
583 M. (2014). Comparative hydrodynamics of 10 Mediterranean lagoons by means of numerical
584 modeling. *Journal of Geophysical Research: Oceans*, 119(4), 2212-2226.
585 DOI:10.1002/2013JC009512